Brass instruments as a cascade of two-port networks: Transfer functions, chain parameters, and power efficiency in theory and practice[a)]

Wilfried Kausel,[1,b)] Alexander Mayer,[1] and James W. Beauchamp[2,c)]

[1]*Department of Music Acoustics, University of Music and Performing Arts, Vienna 1030, Austria*

[2]*Department of Electrical and Computer Engineering, School of Music, University of Illinois at Urbana-Champaign, Champaign, Illinois 61801, USA*

ABSTRACT:

This paper investigates how two-port network theory as a means for system identification can be applied to the analysis of brass instruments. A special focus is placed on the energy conversion efficiency as this is limited by inner damping, which receives much attention by expert players and makers of brasses. Theory suggests that a reconstruction of the 2×2 matrix representing the network requires input impedance and transfer function for two different boundary conditions. Besides the normal case of free sound radiation, instruments are also analyzed with the bell closed by a spherical cap. For this purpose, a customized 3D-printed spherical cap was fabricated and attached to the bell. Four measured spectra and the passivity condition over-determine the set of system equations. It is shown how to take advantage of this freedom when analyzing wind instruments. Measurements and simulations of a trumpet and a trombone are presented and compared.

I. INTRODUCTION

Brass instruments can be modeled as wave guides, in which sound waves move back and forth between the two more or less reflective terminations when excited by an oscillating sound flow at the mouthpiece. Linear wave propagation obeys the same laws and principles, whether it concerns sound waves, electromagnetic waves, or water waves. So it is the same mathematics that has to be applied in all cases.

The most rigorous and systematic treatment of one-dimensional wave propagation has been derived for electrical networks, and sophisticated network simulators have been around since 1975 (Nagel, 1975). In 1982, Elliott used the previously known analogy between sound pressure and flow on one side and electrical voltage and current on the other side to elaborate on the input and transfer response of real brass wind instruments (Elliott *et al.*, 1982). In 1996, Leach simulated horns using the network simulator SPICE (Leach, 1996).

The theory dealing with cascaded wave guides for waves characterized by two wave variables, such as voltage and current or sound pressure and flow, is known as two-port network theory (Gatland, 2016). Wave variables are represented by complex functions of frequency that determine amplitude and phase of some oscillating physical quantity. Wave guides are represented by a two-port network that is described by a 2×2 matrix of four complex functions of frequency, the system parameters, for which several different representations exist. For our purposes, we will focus on the so-called chain parameters $A_{i,j}$ because they allow simple cascading of many elementary two-port networks in order to compose much more complex systems that correspond to the actual bore profile of a real musical instrument.

Cascading is shown in Eq. (1), where sound pressure p_1, sound flow u_1, and input impedance $Z_1 = p_1/u_1$ represent physical quantities related to the left end of an acoustic duct, while p_2, u_2, and termination impedance $Z_2 = p_2/u_2$ represent corresponding quantities related to its right end.

$$\begin{pmatrix} p_1 \\ u_1 \end{pmatrix} = \begin{pmatrix} A_{1,1} & A_{1,2} \\ A_{2,1} & A_{2,2} \end{pmatrix} \cdot \begin{pmatrix} p_2 \\ u_2 \end{pmatrix}. \tag{1}$$

Other important relationships are the input admittance $Y_1 = u_1/p_1$, the termination admittance $Y_2 = u_2/p_2$, the pressure transfer function $T_p = p_2/p_1$, which is often referred to as pressure gain, and the flow transfer function $T_u = u_2/u_1$, which has minor practical significance. Currently available methods of sound flow measurement are less accurate than the sound pressure signals derived from calibrated microphone recordings.

An important constraint when two-port networks according to Eq. (1) are applied to acoustical systems is

related to the "reciprocity theorem." It is thoroughly covered in Rayleigh (1896) (Vol. 1, pp. 150–157), generalized in Carson (1924), and reviewed more recently in Goedbloed (2006). It states that passive linear networks are reciprocal with few exceptions typically concerning external fields or moving fluids. Since the mean flow velocity in brasses is small compared to the speed of sound, such instruments are approximately reciprocal.

In reciprocal systems, the forward and backward transfer admittances are equal. They are given by $Y_{t,fw} = u_2/p_1$ when $p_2 = 0$ and $Y_{t,bw} = -u_1/p_2$ when $p_1 = 0$. When this condition is evaluated for a system described by Eq. (1), the passivity condition

$$Det(A_{i,j}) = A_{1,1}A_{2,2} - A_{1,2}A_{2,1} = 1 \qquad (2)$$

is obtained.

Chain parameters allow easy concatenation of several such two-port networks. The matrix product of all 2×2 matrices $A_{i,j}$ determines the matrix of a composite two-port network inside which all elementary two-port networks have been linearly aligned and connected. The output signals (p_2, u_2) of each cell are the input signals (p_1, u_1) of their right neighbor, and their inputs are driven by the outputs of their left neighbor. This also means that the termination impedance of each element is determined by the input impedance of its right neighbor.

The bore diameter of wind instruments usually varies along their axis. Therefore, they can be decomposed into many short slices of simple cylindrical or conical shape. Each slice or element is represented by a corresponding two-port network. The input impedance of the left-most element is the input impedance of the entire instrument. The termination impedance of the right-most element is the radiation impedance of the entire instrument.

The four matrix elements of each elementary two-port network are complex functions of the angular frequency ω, geometric parameters such as bore diameters and length of the slice, and physical parameters such as air density and viscosity, speed of sound, and temperature. Air viscosity and boundary layer thickness, which is determined by the inner surface roughness, determine the thermo-viscous losses.

Since real instruments are typically composed of hundreds of such elements whose matrices must be multiplied, even small numerical errors accumulate quickly. Enforcing the passivity requirement for each elementary matrix as well as for all intermediate matrix products may reduce simulation quality considerably.

Brass wind instruments are excited in the mouthpiece entry plane by a periodically oscillating acoustic flow signal $u_{in}(\omega)$ generated by the player's oscillating lips. The mouthpiece pressure $p_{in}(\omega)$, which builds up in front of the player's lips inside the mouthpiece, is essential to control and synchronize the lip motion. This pressure is exceptionally high (Beauchamp, 1980; Hirschberg et al., 1996) at resonances of the air column that correspond to strong local maxima

of the input impedance function. Although this can lead to nonlinear propagation, in this paper we only consider linear propagation theory, which is applicable at low performance intensities.

Therefore, the input impedance spectrum of a wind instrument contains information about frequency, strength, and quality factor Q of all air column resonances that can be excited by a player. This means it gives an indication of intonation, responsiveness, and expressiveness of an instrument. And even the radiated sound, which is composed of single harmonic components, is influenced by the fact that some harmonics of the excitation signal—the acoustic flow nonlinearly modulated by the oscillating lip orifice—may be supported by air column resonances, while others may not be.

However, due to the historically great importance assigned to the input impedance function, other relationships are often neglected. Especially the transfer function $T_p(\omega)$ between the sound pressure at the excitation point $p_1(\omega)$ and the sound pressure at the open mouth of the bell $p_2(\omega)$ deserves specific attention. Without this knowledge, it is possible neither to predict the radiated sound nor to assess the power efficiency of brass wind instruments—both being important for musicians and makers when discussing quality aspects.

A. Review of previous work on power efficiency

This research is based on the already mentioned paper by Elliott et al. (1982), who applied electrical network theory to wind instruments by treating trumpets or trombones as acoustical two-port networks. They described such instruments in terms of their input impedance, when terminated by an impedance corresponding to a radiation load at the bell, and by the pressure transfer function, which corresponds to the voltage gain of an electrical circuit.

They also developed expressions for the reflection coefficient at the mouthpiece plane and the power efficiency of a wind instrument. The power efficiency and transfer function relationship were also described by Beauchamp (1988a,b).

With two notable exceptions (Fletcher and Tarnopolsky, 1999; Kausel et al., 2013), acoustic power efficiency has been completely neglected in research since 1982. It is not even indexed in Fletcher and Rossing (1991) or in Chaigne and Kergomard (2016). Therefore, this topic has received a special focus in this paper, and several sections are dedicated to covering it theoretically and experimentally.

Since power efficiency can be obtained experimentally by measuring sound pressure and power at the open mouth of the instrument while simultaneously determining mouthpiece pressure and input impedance, it may also serve to verify theoretical models of the radiation impedance for various boundary conditions. In particular, radiation impedance modeling has remained a weak point in acoustics up to present times because sound radiation strongly depends on the acoustic environment, which is typically far too complicated for an analytical model. Output measurements with

J. Acoust. Soc. Am. **149** (4), April 2021

Kausel et al. 2699

calibrated microphones in an anechoic chamber are necessary to minimize these complications.

Analytical expressions for the radiation impedance have been presented by Crandall (1926) and Bauer (1944) for the case of a pulsating sphere in free space, by Zorumski (1973) for the case of a circular or annular flat and rigid piston embedded in an infinite baffle, by Levine and Schwinger (1948) for the case of an unbaffled circular or annular piston, and finally by Helie and Rodet (2003) for the case of a pulsating portion of a sphere in free space. Zorumski had already worked out a multi-modal decomposition for his case in 1973, while all other results have been obtained for the first planar mode or the first spherical mode for cases of spherical symmetry.

B. Outline of this paper

In Sec. II, we first deal with the theory of acoustic two-port networks and with the reconstruction of unknown chain parameters from their known boundary conditions. It will be shown how wind instruments can be measured in order to numerically identify their system matrices.

The next topic in Sec. II is the effective power efficiency of brass wind instruments and how it is related to physical quantities that can be obtained by numerical simulations or by measurements. A practically useful method is proposed for determining this quality-related characteristic of wind instruments experimentally, with and without having an anechoic chamber at one's disposal.

Since radiation impedance has a very strong impact on power efficiency and a less pronounced influence on an instrument's input impedance, it is also studied in detail. Different models are presented and compared. Finally, it is shown how different radiation models affect the reflection coefficient at the open mouth of the bell. This comparison reveals a fundamentally different behavior for frequencies above a certain cutoff frequency.

Section III presents actual measurements for a typical B♭-trumpet. Resulting chain matrix parameters will be presented and discussed. Some focus has been put on the passivity condition and how it can be used to determine the quality of real world measurements.

Similar measurements and reconstruction results of a popular plastic tenor trombone, the "PBone," were also completed but could not be included in this article due to space limitations. They can be accessed in the research data repository linked to this paper.[1]

Section IV deals with the effective power efficiency of brass wind instruments and how it can be derived in several different ways from impedances and pressure gains obtained either by measurements or by physical modeling. Results for the trumpet and for the trombone are presented and compared with simulation results based on lossy and more or less lossless wave guide models.

Section V summarizes the results and what has been learned from comparing various ways to measure and analyze acoustical systems, namely brass wind instruments, and to assess their quality.

II. TWO-PORT NETWORK THEORY

Two-port networks can be used for modeling linear one-dimensional wave propagation. They can be represented by a 2×2 matrix of four parameters. This matrix propagates the wave state vector (p_2, u_2) from the output back to the input as (p_1, u_1). This propagation as shown in Eq. (1) corresponds to an equation system of two coupled equations.

If the wave states at both the output and the input are known for two different operating conditions, four coupled but independent equations can be obtained to determine the four unknown matrix parameters of the system. This procedure is called *system identification*.

Passive systems are systems that only dissipate and do not generate energy. For such systems, Eq. (2) must be fulfilled. Since acoustical systems without any active components can only be passive, there is consequently a fifth equation available for system identification.

This allows us to replace one of the measurements by the passivity condition. Therefore, the measurement that is most difficult or least accurate can be omitted. Below it is also shown how to benefit from this redundancy when the power efficiency of an instrument is to be determined experimentally.

A. Transmission system identification

In electrical engineering, it is common practice to determine unknown inner network parameters by measuring the voltages v_1 and v_2 as well as the currents i_1 and i_2 at ports 1 and 2 for two different operating conditions. Typically, one of these cases is a short circuit where the output port is loaded by an infinitesimally small resistance, thus enforcing zero output voltage $v_2 = 0$. The other case is the so-called idle case or open circuit, where no output load is applied, which enforces zero output current $i_2 = 0$.

There is no acoustical equivalent of the short circuit. Maximum flow and minimum sound pressure occur when an instrument's bell is open to an anechoic environment. The idle case has an acoustical equivalent that can be realized and measured. It is a solid and air-tight termination at the rim of the bell. A perfectly reflecting wall enforces zero sound flow and maximum sound pressure. Since wave fronts in flaring bells are approximately spherical, the ideal termination should follow this shape. We used a 3D-printed spherical cap rigidly coupled to the rim as shown in Fig. 1. Its sphere radius was chosen to let the cap touch the rim perpendicularly to the wall.

Sound pressure signals in the mouthpiece entry plane p_1 as well as in the bell exit plane p_2 can be recorded using calibrated measurement microphones. Their ratio p_2/p_1 is called the sound pressure transfer function, T_p. Often, it is also referred to as *pressure gain*.

Acoustic input impedance measurement methods are well established (Dalmont, 2001; Dickens *et al.*, 2008;

2700   J. Acoust. Soc. Am. **149** (4), April 2021

Kausel *et al.*

Keefe *et al.*, 1992), and several practical setups are in widespread use. Input impedance is defined as $Z_1 = p_1/u_1$ and input admittance as $Y_1 = u_1/p_1$.

Radiation impedance $Z_{rad} = Z_2 = p_2/u_2$ does not depend on the internal bore profile of the instrument and may therefore be theoretically determined instead of actually measured. There are several useful models for this radiation impedance if anechoic conditions can be assumed and the last bore diameter of the open mouth of the bell is known.

Unfortunately, the radiation impedance Z_{rad} non-negligibly affects the input impedance Z_1. This means that the actual radiation impedance of the horn during measurement contributes to the measured input impedance but is not taken into account by the simplified theoretical model used in system reconstruction. This inconsistency can be avoided if the passivity condition $Det(A_{i,j}) = 1$ is used instead of including the theoretical radiation impedance in the system reconstruction.

The actual system identification equations for two arbitrarily different operating conditions [1] and [2] can be derived from Eq. (1) and the definitions for Z_1, Z_2, and T_P according to

$$A_{1,1} = \frac{Z_2[1]T_p[2] - Z_2[2]T_p[1]}{(Z_2[1] - Z_2[2])T_p[1]T_p[2]}, \tag{3}$$

$$A_{1,2} = \frac{Z_2[1]Z_2[2]\big(T_p[1] - T_p[2]\big)}{(Z_2[1] - Z_2[2])T_p[1]T_p[2]}, \tag{4}$$

$$A_{2,1} = \frac{\dfrac{Z_2[1]}{Z_1[1]T_p[1]} - \dfrac{Z_2[2]}{Z_1[2]T_p[2]}}{Z_2[1] - Z_2[2]}, \tag{5}$$

$$A_{2,2} = \frac{Z_2[1]Z_2[2]\big(Z_1[1]T_p[1] - Z_1[2]T_p[2]\big)}{Z_1[1]Z_1[2](Z_2[1] - Z_2[2])T_p[1]T_p[2]}. \tag{6}$$

These expressions can be simplified if operating case [1], the "closed" case, is characterized by perfect reflection at the end of the flaring bell and case [2], the "open" case, is characterized by free field radiation, where $Z_2 = Z_{rad}$ according to some physical model. In the former case, radiation is blocked by a perfectly reflecting spherical cap that

FIG. 1. (Color online) 3D-printed spherical cap with microphone for pressure gain measurements in closed state.

must be air-tightly attached to the rim. This enforces $u_2 = 0$, $Z_2 = \infty$, $Y_2 = 0$ and perfect wave reflection with a reflection coefficient $R_2 = 1$.

With simplified notation (T_{cl}, T_{op} for $T_p[1]$, $T_p[2]$ and Z_{cl}, Z_{op} for $Z_1[1]$, $Z_1[2]$), the system identification terms are now given by

$$A_{1,1} = \frac{1}{T_{cl}}, \tag{7}$$

$$A_{1,2} = Z_{rad}\left(\frac{1}{T_{op}} - \frac{1}{T_{cl}}\right), \tag{8}$$

$$A_{2,1} = \frac{1}{T_{cl}Z_{cl}}, \tag{9}$$

$$A_{2,2} = Z_{rad}\left(\frac{1}{T_{op}Z_{op}} - \frac{1}{T_{cl}Z_{cl}}\right). \tag{10}$$

If Z_{rad} is not to be modeled but derived from the passivity condition, it can be substituted (with $Y_{cl} = 1/Z_{cl}$ and $Y_{op} = 1/Z_{op}$) as

$$Z_{rad} = \frac{T_{cl}T_{op}}{Y_{op} - Y_{cl}} = \frac{1}{Y_{rad}}. \tag{11}$$

With this substitution in Eqs. (7)–(10), the system matrix can now be reconstructed from the basic set of measurements without the need for a physical model of the radiation impedance. Pressure p and flow u are therefore propagated according to

$$\begin{pmatrix} p_1 \\ u_1 \end{pmatrix} = \begin{pmatrix} \dfrac{1}{T_{cl}} & \dfrac{T_{op} - T_{cl}}{Y_{cl} - Y_{op}} \\ \dfrac{Y_{cl}}{T_{cl}} & \dfrac{T_{op}Y_{cl} - T_{cl}Y_{op}}{Y_{cl} - Y_{op}} \end{pmatrix} \cdot \begin{pmatrix} p_2 \\ u_2 \end{pmatrix}. \tag{12}$$

It should be emphasized that this method for system identification is also free from any assumption about the actual radiation impedance. Therefore, it is not necessary to make the measurements for the open operating case under anechoic conditions. Any room with a reasonably dry acoustics will do.

However, care should be taken to do the input impedance measurement either simultaneously or at least with the exact same position of the bell with respect to the room and without changing the ambient acoustics by moving absorbing or reflecting elements, e.g., opening or closing doors or windows, between the two measurements for the open case.

The actual radiation impedance will then affect the input impedance and the pressure transfer function in exactly the same way and so will cancel out in the derivation of the system matrix coefficients. These coefficients are properties of the wave guide itself and independent of the boundary condition that has been chosen for the open case.

But there is an alternative way to incorporate the passivity condition in the system identification process. Instead of eliminating the radiation impedance model, the free field

measurement of the pressure transfer function T_{op} can be obviated.

For any assumption of the actual radiation impedance Z_{rad}, the free field transfer function T_{op} can be calculated according to

$$T_{op} = \frac{Z_{rad}(Y_{op} - Y_{cl})}{T_{cl}}, \qquad (13)$$

based on the passivity condition. In this case, a complete system identification only requires the three measurements Y_{op}, Y_{cl}, and T_{cl} and a theoretical model for Z_{rad}. An example for such a reconstruction is given in Sec. III. The advantage of this approach is that none of the measurements has to be made in an anechoic chamber.

However, all these system identification methods rely on an ideal closed condition. Here, it is essential that nearly perfect reflection takes place at the spherical cap terminating the bell. The slightest leakage will have strong impact on the amplitudes of low frequencies. Mechanical resonances of the cap have critical influence wherever they occur. If the assumption that the reflection coefficient of the cap $R_2 = 1$ is violated and some non-zero wall admittance leads to incomplete reflection, the resulting matrix coefficients will not be perfect.

B. Power efficiency

The efficiency of an instrument can be calculated by relating the radiated effective sound power at the open bell to the effective sound power supplied by the player. It is mainly determined by viscous losses in the boundary layer of a wind instrument.

Efficiency is a quality-related parameter that receives a lot of attention from players because of its suspected impact on the sound timbre, the responsiveness, the pitch flexibility, and the air volume required to hold long notes. However, there is a still ongoing debate about whether and how such subjective assumptions can be correlated with objective physical characteristics of brass wind instruments (Campbell, 2004).

Sound waves that are radiated quickly will experience less frictional losses as compared to waves that recirculate many times inside the resonant air column before eventually being radiated (Elliott and Bowsher, 1982). Recirculation requires reflection at the open mouth of the instrument.

The shapes of brass wind instrument bells enable the reflection of sound waves rather well, at least up to the so-called cutoff frequency, which is not a sharp frequency but rather a transition band. An expression for this frequency, below which the first non-planar mode is evanescent, in terms of the horn function U and the speed of sound c has been derived by Jansson and Benade (1974). A slightly different version depending on the bell radius b has been used here. In Braden (2006) and more recently in Campbell et al. (2020) (p. 211), it is given for the plane wave mode as

$$f_{cutoff} > 1.84 \frac{c}{2\pi b}. \qquad (14)$$

Consequently, power efficiency above the cutoff frequency can be expected to be much higher compared to the lower playing frequency range where resonances are strongest and reflectance at the flaring bell is closest to 1.

Boundary layer losses are affected by the surface condition (Berggren et al., 2018) and the mechanical admittance of the wall (Kausel et al., 2010; Moore et al., 2015; Watkinson and Bowsher, 1982). Additional losses due to turbulence, modal conversion, and evanescent waves are related to discontinuities in the bore profile (Braden, 2006; Kemp, 2002). The reflectance of the bell depends on its shape (Campbell et al., 2013) and on the actual radiation impedance, which is determined by the acoustics of the environment.

Power efficiency E is given by

$$E = \frac{P_{out}}{P_{in}} = \frac{|p_2|^2 Re(Y_{rad})}{|p_1|^2 Re(Y_{op})} = |T_{op}|^2 \frac{Re(Y_{rad})}{Re(Y_{op})}, \qquad (15)$$

with P_{out} and P_{in} being the effective output and input powers (Elliott et al., 1982). p_2 and p_1 are again the complex sound pressure amplitudes in the tube exit plane—or rather where the axis intersects the spherical wave front when it passes the rim—and in the center of the mouthpiece entry plane. Their ratio defines the pressure gain T_p for particular boundary conditions. $Re(Y_{rad})$ and $Re(Y_{op})$ are the real parts of the complex free field radiation and its associated input admittance, i.e., the reciprocals of the complex radiation and input impedance, respectively.

Since the radiation admittance $Y_{rad} = 1/Z_{rad}$ depends strongly on the environment and cannot be measured easily, its measurement is often replaced by a theoretical model. Such models will be discussed in Sec. II D.

But if it is possible to measure input impedance Z and pressure gain T not only in the open but also in the closed case, then any assumption about the radiation conditions can be avoided. According to Eq. (11), Y_{rad} can be substituted by a term that is based on the passivity condition and only depends on known and measurable quantities.

Since this expression for the power efficiency is now free from any assumption of a specific radiation impedance, it can be applied to real life environments and is no longer restricted to free field conditions. An anechoic chamber is no longer required if the terms are met that have already been mentioned in the context of Eq. (12).

But it should be pointed out that power efficiency, unlike the system matrix coefficients treated above, is not only a property of the network itself but also of its load condition, even though it is strongly influenced by internal losses of the two-port network.

In the closed case, power efficiency has to be zero because there is no radiated sound power p_2. All the input power is dissipated inside the network, which makes it possible to measure these losses directly.

By measuring input impedance and pressure gain for several extremely different room acoustics, such as in an anechoic chamber and a reverberation room, it is possible to study the influence of the environment on the playing conditions faced by the player.

C. Efficiency measurement using far field pressure

It should be noted here that under certain assumptions, there is an alternative way to determine the power efficiency. Instead of measuring the output pressure at the bell plane, it is possible to measure the pressure in the far field by placing the output microphone a suitable distance from the bell on axis. This would work for instruments such as the trumpet and the trombone having a single radiation output port and a well defined radiation axis. In that case, the output power is given by

$$P_{out} = 4\pi d^2 D(\omega)\frac{p_{rms}^2}{Z_0}, \tag{16}$$

where d is the distance from the bell to the microphone, $D(\omega)$ is a frequency-dependent directivity index, and $Z_0 = \rho_0 c$ is the characteristic acoustic impedance of air (Molloy, 1948). The efficiency determined using a microphone at some distance d for measuring the pressure gain $T_{p,ff}$ from the mouthpiece entry plane to the far-field can then be written as

$$E(\omega) = \frac{4\pi d^2}{Z_0}D(\omega)\frac{T_{p,ff}^2(\omega)}{Re(Y_{in}(\omega))}. \tag{17}$$

The far-field measurement has the advantage that the radiation admittance does not need to be known or measured. However, because of difficulties with microphone placement, requirements for far-field measurements in an anechoic chamber and challenges in estimating $D(\omega)$ for frequencies above cutoff, it is more practical to use the methods described in Sec. II B, which do not require knowledge of the radiation admittance.

D. Radiation impedance models

As already stated, there have been several attempts to describe the radiation impedance for different idealized conditions. For one-dimensional wave guide models, two are of

specific interest and will be reviewed in greater detail below. The Levine–Schwinger (Levine and Schwinger, 1948) result is accurate for nearly cylindrical structures where plane wave propagation can fairly be assumed. For flaring bells, this assumption is certainly not valid. There the radiation wave front is definitely not planar, and the spherical approximation developed by Helie–Rodet (Helie and Rodet, 2003) is a much more accurate approximation.

The model of Zorumski (1973) requires an infinite baffle, which does not exist in the usual case. It therefore deviates significantly from reality. However, as it employs modal decomposition, it is the only existing model that can be used in multi-modal simulations (Braden, 2006).

A comparison between four different radiation impedance models applied to the B♭-trumpet bell with 12.3 cm bore diameter, a cutoff frequency of 1630 Hz, and a maximum flare angle at the rim with $\tan(\theta) = 3.23$ has been plotted in Fig. 2. The mathematical representation of these models will be elaborated in Secs. II D 1–II D 3.

It can be seen in these impedance graphs that only two of the most popular radiation models, the models by Elliott and Helie–Rodet, do not completely fail above the cutoff frequency. Both implement a kind of saturation, which corresponds to the expected behavior in this frequency range.

Figure 3 shows quite well how the reflection coefficient at the open mouth of the bell is influenced by this crucial behavior of the radiation model. While real bells only reflect below cutoff, some models such as the ones by Levine–Schwinger and Braden completely neglect this physical reality.

The Crandall (1926) model mentioned by Bauer (1944) as well as the model by Zorumsky have not been considered. Their modeling accuracy for unbaffled bells radiating under free field conditions is simply not satisfactory.

1. Levine–Schwinger approximation

Levine and Schwinger (1948) derived an integral formulation of the pressure reflection coefficient R at the open end of an unflanged cylindrical tube. This approximation for the first planar mode is only valid below the cutoff frequency of all higher modes (Silva et al., 2009). The radiation impedance Z_{rad} can be expressed in terms of the reflection coefficient R, the wave number k, and the acoustical length L as
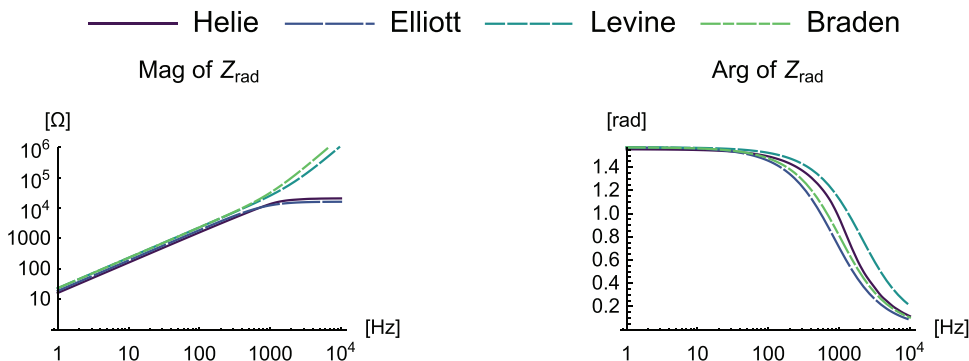

FIG. 2. (Color online) Complex termination impedance of a trumpet bell according to four different radiation models.
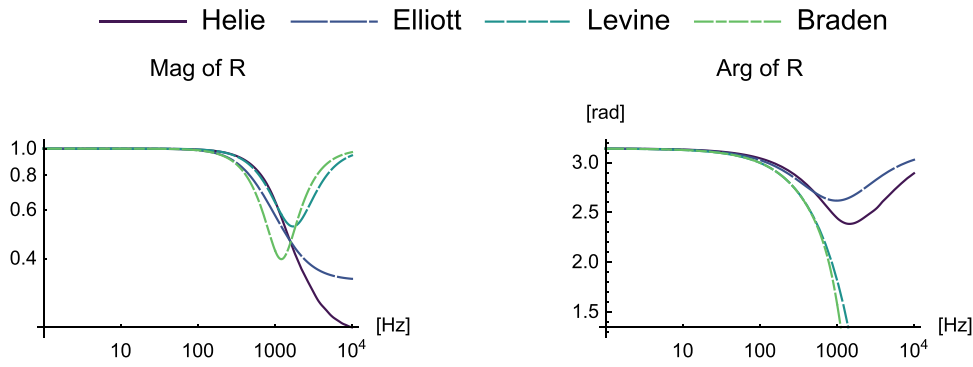
J. Acoust. Soc. Am. **149** (4), April 2021

Kausel et al.   2703

FIG. 3. (Color online) Complex reflection coefficient of a trumpet bell according to four different radiation models.

$$Z_{rad} = \frac{1+R}{1-R} = -j\tan\left(kL - j\frac{1}{2}\ln|R|\right). \tag{18}$$

A commonly used numerical fit of this expression ignoring powers of k beyond k^2 was given in Nederveen (1969) [Eq. (22.14)] according to

$$Z_{rad} = \frac{k^2\rho c}{4\pi} + j\frac{6133 k\rho c}{10000\pi b} \tag{19}$$

with a real part of the corresponding admittance of

$$Re(Y_{rad}) = \frac{2500\pi c b^2}{3721\rho c^2 + 2500\pi^2 f^2 b^2 \rho}, \tag{20}$$

where b is the radius of the circular opening, c the speed of sound, ρ the air density, and f the frequency.

2. Elliott et al. approximation

In their seminal paper, "Input and transfer response of brass wind instruments," Elliott *et al.* (1982) gave an expression for Y_{rad} according to

$$1/Z_{rad} = \frac{2\pi b^2}{\rho c} + \frac{2\pi b}{j\omega\rho}, \tag{21}$$

where b is the bell radius, c the speed of sound, ρ the air density, and $\omega = 2\pi f$ the angular frequency and the imaginary unit $j = \sqrt{-1}$.

This can be rearranged to obtain Z_{rad} with the real and imaginary part in separate terms:

$$Z_{rad} = \frac{2\pi c f^2 \rho}{c^2 + 4\pi^2 f^2 b^2} + \frac{jc^2 f\rho}{b(c^2 + 4\pi^2 f^2 b^2)}. \tag{22}$$

Braden (2006) combined the real part from Elliott without the saturation term at cutoff and took the imaginary part from the simplified Levine–Schwinger model according to Nederveen, ending up with

$$Z_{rad} = \frac{2\pi f^2 \rho}{c} + j\frac{6133 f\rho}{5000 b}, \tag{23}$$

which is almost identical to Eq. (19) except for a factor of 2 in the real part. If this came in by mistake, it has not been

spotted yet, since the real part does not make much difference in the frequency range where those models are usually applied.

3. Helie–Rodet approximation

The approach of Helie and Rodet is based on spherical wave propagation, which more realistically matches the conditions at the end of the bell of a typical brass wind instrument. The exit wave front is treated as a pulsating portion of a sphere radiating into an anechoic 3D environment with no baffle (Helie and Rodet, 2003).

Unfortunately, even the numerical evaluation of this result is quite demanding, as it is represented by a slowly converging sum of terms involving spherical Hankel functions h_n as well as Legendre polynomials P_n of high order N. Helie and Rodet calculated the sum with $N = 200$ terms. Here, $N = 60$ terms have been used, which is sufficiently accurate up to 10π times the cutoff frequency. This is more than 16 kHz for most cases. With θ being the flare angle and $\nu = fb/c = f/(\pi f_{cutoff})$ the normalized frequency, a normalized radiation impedance $Z_{rad}^* = Z_{rad}/Z_o$ (Z_o being the characteristic specific impedance ρc) is given by

$$Z_{rad}^* = -\frac{2j}{1 - \cos(\theta)}\sum_{n=0}^{N}\frac{\gamma(n, 2\pi\nu)\mu(n, \theta)^2}{2n+1}, \tag{24}$$

with

$$\mu(n, \theta) = \frac{1}{2}\left(P_{n-1}(\cos(\theta)) - P_{n+1}(\cos(\theta))\right) \tag{25}$$

and

$$\gamma(n, \omega) = \frac{\omega h_n^{[2]}(\omega)}{n h_n^{[2]}(\omega) - \omega h_{n+1}^{[2]}(\omega)}. \tag{26}$$

The expression for the radiation impedance Z_{rad} for real frequencies f, bell radius b, speed of sound c, and density ρ becomes

$$Z_{rad} = -\frac{j2\rho c}{1 - \cos(\theta)}\sum_{n=0}^{N}\frac{\gamma\left(n, 2\pi f\frac{r}{c}\right)\mu(n, \theta)^2}{2n+1}. \tag{27}$$

Of course, $Re(Y_{rad})$ is calculated by taking the real part of the reciprocal of Z_{rad}. Although it might appear that Z_{rad}, and thus Y_{rad}, is purely reactive, in fact they have real parts because the h Hankel functions and thus the γ values are complex.

Since this model as described above is numerically extremely expensive if not infeasible for practical applications, an interpolation between precomputed normalised impedance values for flare angles between $5°$ and $90°$ and a normalized frequency up to 10 times the cutoff frequency has been used. Alternatively, the second order high-pass filter approximation proposed by Eveno *et al.* (2012) could have been used.

E. Reflection coefficient of a trumpet bell

The reflection coefficient R at the open end of an infinitely long tube is given by

$$R = -\frac{Z_{rad} - Z_c}{Z_{rad} + Z_c} \qquad (28)$$

with the characteristic impedance $Z_c = \rho c/(b^2 \pi)$, where ρ is the air density, c the speed of sound, and b the bell radius. Z_{rad} can be modeled by any of the approximations given in Sec. II D.

Graphs of R vs frequency for a circular cross section of 12.3 cm, which corresponds to our sample B♭-trumpet, are shown in Fig. 3. The behavior beyond cutoff is especially interesting. Only the model by Helie and Rodet follows the expected downward radiation curve beyond cutoff. Elliott is close, but its reflectance beyond cutoff is much too large.

III. NUMERICAL AND EXPERIMENTAL DETERMINATION OF NETWORK PARAMETERS

Acoustical input impedance and sound pressure gain are complex functions of frequency that can either be determined by means of physical modeling—if bore profile and termination conditions are known—or through measurements. To prove the feasibility of the proposed system identification approach, both have been done for comparison purposes.

For this paper, a straight cylindrical tube and two different brass wind instruments, a B♭-trumpet and a tenor trombone, have been analyzed experimentally and numerically. Simulations have been done with a lossy and a lossless wave guide model and with three different radiation impedance approximations. Besides that, there are three possible system identification strategies that have all been tested and compared.

Space does not allow sharing all of these data in printed form. Some of the most essential graphs are given here. But the whole wealth of data will be available in an open online repository together with the Mathematica Notebook[1] that was used for all derivations, for simulations, and for creating the plots.

The wave guide model that was implemented in Mathematica is the one described by Mapes-Riordan (Kausel, 2004; Mapes-Riordan, 1993). It takes thermoviscous losses in the boundary layer into account. For the lossless simulations, all loss related terms have been scaled down by 10^{-6}. Zeroing all such terms turned out to cause numerical problems.

Measurements were made in the anechoic chamber of the first two authors' institution using the BIAS impedance analysis system (ARTIM, 2021). Bore profiles of both instruments have been mechanically measured and subsequently adjusted for an acceptable match between simulated and measured input impedance curves by means of computer optimization (Kausel, 2004). These bore profiles are also available in the data repository of this publication.[1]

A. B♭-trumpet two-port network parameter identification

Figure 4 shows graphs of measured input impedance magnitude and phase vs frequency and pressure transfer function magnitude and phase vs frequency for the open and closed cases. Measurements for the open case have been made under free field conditions. The vertical grid lines show the position of all resonances of the open instrument. They may serve as a helpful indication for the interpretation of other plots.

Surprisingly, the natural tones especially in the low register are not much affected in pitch when the termination impedance is switched from the open condition to the completely closed one. This is very much different from the behavior of a straight tube. It shows that the sensitivity of the input impedance to variations in the termination impedance is rather low. Otherwise, mutes could not be used in live performance.

This low sensitivity to the conditions at the far end has another advantage. It allows accurate measurements of the input impedance outside an anechoic chamber. Therefore, input impedance measurement heads are not only useful for scientific labs but also for instrument makers and repair shops.

Thus, it turns out that the only measurement that really needs free field conditions is the sound pressure transfer function, also called the pressure gain. But as there are five equations determining four system parameters, the pressure transfer function for the open case can be computed using the passivity condition, which led to Eq. (13).

The measured and such a "synthetic" free field pressure gain under the assumption of perfect radiation according to Helie–Rodet can be compared in Fig. 5. It can be seen that the synthetic T_{op} based on the passivity condition shows reduced loss up to about 1700 Hz. Possible reasons contributing to this difference could be distance, centering, or gain of the near field microphone or a mismatch between the radiation model and the actual radiation conditions.

Beyond cutoff (around 1600 Hz), there is also some disagreement between the curves. This is most probably due to the radiation model, which is a necessary assumption for the

J. Acoust. Soc. Am. **149** (4), April 2021
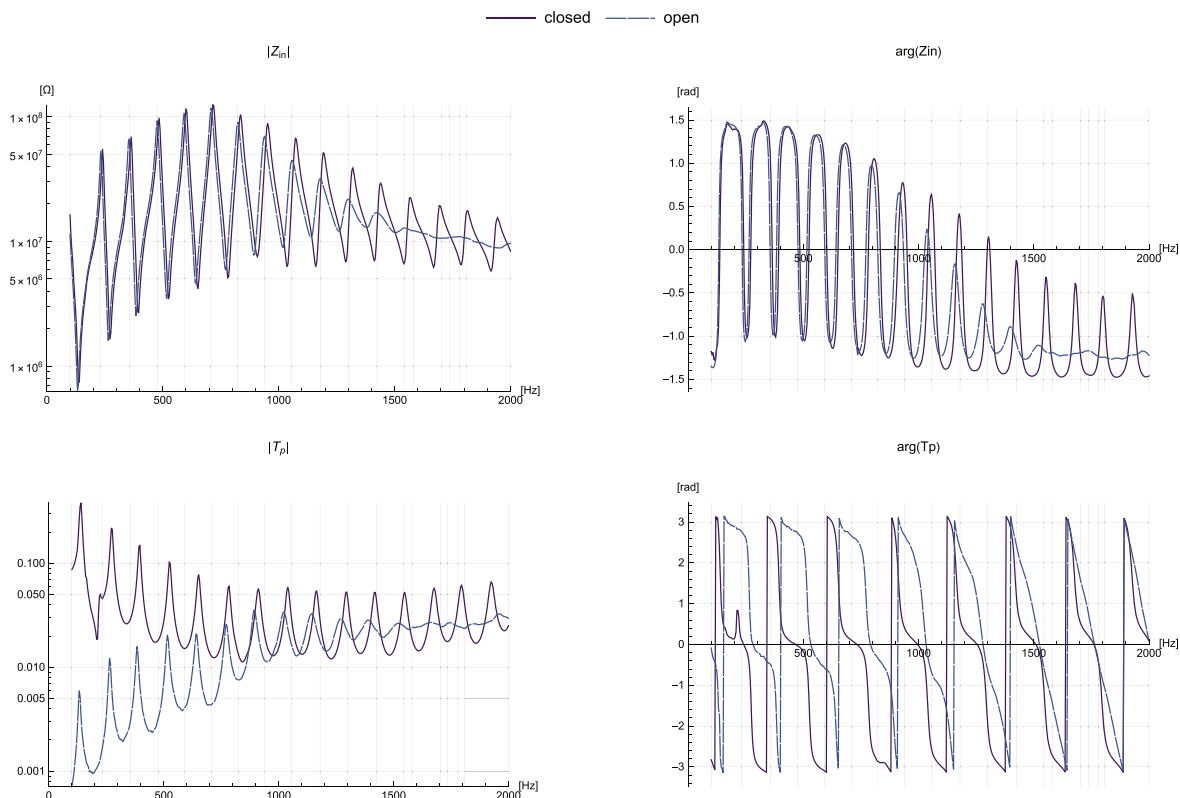
Kausel *et al.*   2705

FIG. 4. (Color online) Complex input impedance and pressure gain of a B♭-trumpet, open and closed, as measured for system identification purposes.

synthetic curve. It is known that radiation models are primarily useful below cutoff, and even the one by Helie–Rodet starts to deviate from the physical reality at higher frequencies.

The error in the synthetic T_{op} around 200 Hz was caused by a mechanical resonance of the reflecting cap. Such artifacts mainly affect the pressure gain measurement in closed mode T_{cl}, and this is directly proportional to the reconstructed radiation impedance in Eq. (11), indirectly proportional to the synthetic transfer function T_{op} in Eq. (13), and affects the system matrix coefficients $A_{i,j}$ according to Eqs.

(7)–(10) and (12). This can be seen in the magnitude vs frequency plots shown in Fig. 6.

Except for the above mentioned problems around 200 Hz, there is good agreement between the reconstructed system matrix coefficients and the wave guide theory. This is important because it is this very system matrix that carries all the information about how the instrument propagates acoustic waves in both directions for any possible boundary condition that can be enforced practically or theoretically.

If someone is interested in the intonation of this trumpet, he only needs to specify the termination conditions on
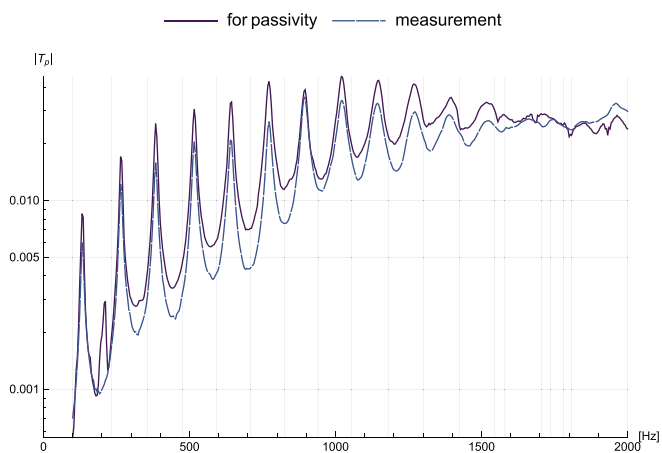

FIG. 5. (Color online) B♭-trumpet pressure gain magnitude vs frequency, as measured under free field conditions and as would be enforced by passivity condition.
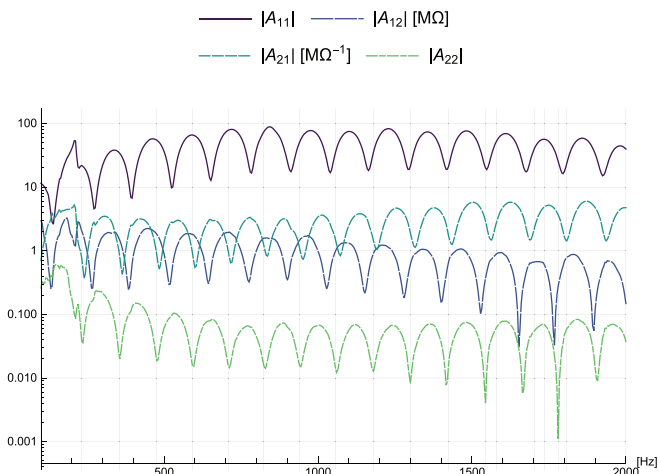

FIG. 6. (Color online) Magnitudes of system matrix coefficients of the B♭-trumpet as reconstructed using above set of four basic measurements.

both ends—e.g., free field radiation at the bell and perfect reflection at the mouthpiece—to be able to calculate input impedance, sound pressure gain, or power efficiency.

If someone wants to know whether Beethoven would have been able to use this trumpet as a hearing aid, he might calculate the sound pressure gain from the open bell back to the mouthpiece plane when this is terminated by the input impedance of a human ear canal.

It should therefore be clear that no cutoff region can be seen in the system matrix, because this property is based on the reflection coefficient at the bell, which depends on the mismatch between the output impedance of the instrument and the termination impedance at the bell. In the closed case or even with some kind of mute, the cutoff region will no longer be where Eq. (14) would predict.

A complete set of experimental and theoretical results not only for the trumpet but also for a trombone can be downloaded from the data repository that accompanies this publication.[1]

The radiation impedance Z_{rad} that terminates the bell during the measurements for the open case is the only free parameter in Eqs. (7)–(10) if Z_{op}, Z_{cl}, T_{op}, and T_{cl} have been determined experimentally. Therefore, it can be reconstructed according to Eq. (11). The result for the trumpet bell in comparison with some common theoretical models is shown in Fig. 7.

Using this reconstructed radiation impedance and all four basic measurements, the determinant of the system matrix was plotted vs frequency to cross-check for system passivity. As expected, the determinant was constant and real and had a magnitude of 1.

This is not the case if the four basic measurement spectra are combined with one of the theoretical radiation impedance models. To demonstrate the deviation of even a carefully measured system from a perfectly passive one, $Det(A_{i,j})$ as derived from the four measured spectra and the free field radiation model by Helie–Rodet is shown in Fig. 8.
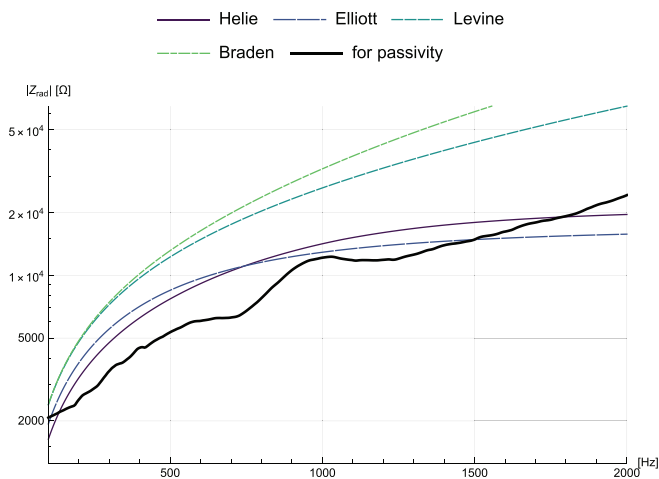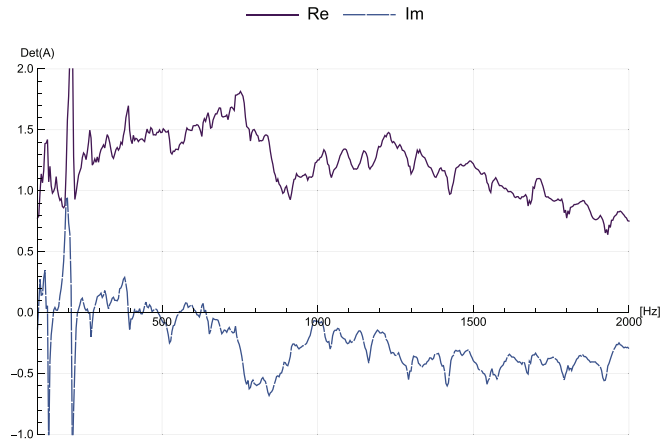

FIG. 8. (Color online) Complex determinant of system matrix of B♭-trumpet reveals some deviations from passivity when the ideal radiation model by Helie–Rodet is combined with a complete set of basic measurements.

The determinant shows significant deviations from 1 around the cap resonance of 200 Hz and beyond cutoff, where the radiation model starts losing its validity. Although there is obviously considerable noise in the remaining regions due to the high numerical sensitivity of the determinant, running averages of the real and imaginary parts are not far from their expected values of 1 and 0. However, these deviations indicate quite well that no anechoic chamber is completely free from spurious standing waves and unwanted reflections.

Nevertheless, this result emphasizes the recommendation given in this paper of including the passivity condition in the analysis and of reconstructing the radiation impedance rather than modeling it for the purpose of system identification and power efficiency analysis.

IV. POWER EFFICIENCY IN THEORY AND PRACTICE

The power efficiency according to Eq. (15) requires knowledge of input admittance, pressure gain, and radiation admittance. Once an appropriate free-field radiation model such as those reviewed in Sec. II D has been selected, input impedance and pressure gain of a given bore profile can be calculated by physical modeling.

The model used for generating the theoretical efficiency curves that have been plotted along with corresponding curves based on actual measurements is a standard one-dimensional transmission-line model for cylindrical and conical bore segments as described by Mapes-Riordan (Kausel, 2004; Mapes-Riordan, 1993). It works equally well for cylindrical elements with plane wave propagation and conical elements with spherical wave fronts. Since the flaring bell is more naturally approximated by conical elements propagating spherical wave fronts, a spherical radiation model such as the one by Helie and Rodet (2003) appears to be suitable.

The instrument itself from the mouthpiece to the bell is composed of a series of conical elements, each one being characterized by a complex frequency dependent 2×2

FIG. 7. (Color online) Magnitude of actual radiation impedance of B♭-trumpet as reconstructed from basic set of measurements and the passivity condition, compared to four theoretical free field radiation models.

J. Acoust. Soc. Am. **149** (4), April 2021

Kausel *et al.* 2707

matrix that propagates the pressure and flow conditions from its right port to its left port. All matrices are multiplied from right to left to obtain an overall system matrix that relates a normalized termination condition at the bell given by $p_2 = Z_{rad}$ and $u_2 = 1$ to some p_1 and u_1 at the mouthpiece entry plane. The resulting ratio $Z_1 = p_1/u_1$ is independent of the normalization, just as is the pressure gain $T = p_2/p_1$.

This can be done not only for the open condition but also for the closed condition characterized by $p_2 = 1$ and $u_2 = 0$. The model contains a thermo-viscous loss term approximating the friction losses in the boundary layer of an air-filled acoustic tube with rigid and perfectly smooth walls.

Zeroing this loss term is problematic because this would create resonances with infinitely high impedance magnitudes. But for studying the loss dependence of the resulting efficiency, these loss terms have successively been scaled down to eventually approach the limit of zero. It is clear that the efficiency of an instrument with zero inner loss must approach 100% at all frequencies.

It is the thermo-viscous losses that cause the efficiency of any acoustical pipe to be less than unity. Below the cutoff frequency, most sound power is reflected by the bell, and only a very small part is radiated. Boundary layer losses will therefore contribute most strongly at low frequencies when waves recirculate very often before a remaining rest is radiated. Above cutoff, there is almost no recirculation, and waves pass only once. Remaining boundary layer losses slightly increase with frequency.

A. B♭-trumpet power efficiency from measurements

The power efficiency of the trumpet as derived from the two measurements Y_{op} and T_{op} according to Eq. (15) has been plotted in Fig. 9. This derivation is based on the assumption of free field radiation as described by the model of Helie–Rodet.

Already discussed weaknesses of this model above cutoff lead to an apparent efficiency of slightly greater than 100% in the corresponding frequency range. This ugly result can be improved by using an efficiency calculation that does not depend on any approximation for the radiation impedance.

Such a formula exists, but it comes at the extra cost of two more measurements. Replacing Y_{rad} according to Eq. (11) requires knowledge of the input impedance Z_{cl} and the pressure gain T_{cl} under closed conditions. The power efficiency corresponding to this method is shown in Fig. 10. This time passivity is enforced, and no efficiency values greater then 100% can occur.

There is also the possibility to derive the power efficiency from only three measurements and the passivity condition. It makes sense to omit the free field sound pressure transfer function if no anechoic chamber is available. The efficiency can then be based on the input impedances Z_{op} and Z_{cl} and the pressure gain T_{cl} in closed mode.
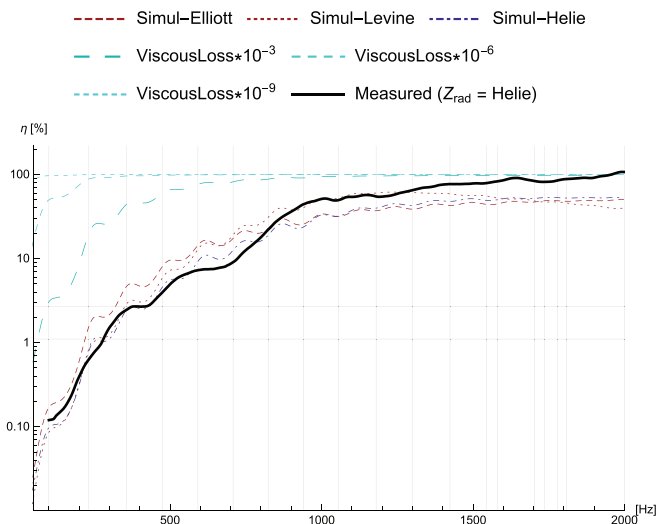

FIG. 9. (Color online) B♭-trumpet efficiency as derived from basic set of measurements and a radiation impedance according to Helie–Rodet, compared to simulations with different radiation models and loss factors.

The substitution according to Eq. (13) can be applied, but now Z_{rad} from one of the models comes again into play. When this substitution is made and Helie–Rodet radiation is again assumed, the curve shown in Fig. 11 is obtained.

Although the passivity condition has been used instead of a measured free field transfer function, there is still the possibility of exceeding the 100% efficiency limit due to a possible mismatch between the radiation impedance of the model and the conditions that were present during the input impedance measurement. By means of the passivity condition, either T_{op} or Z_{rad} can be saved but unfortunately not both.

Finally, Fig. 12 shows the comparison between theoretical and experimental power efficiency curves of the trumpet and the trombone. All other plots for the trombone are
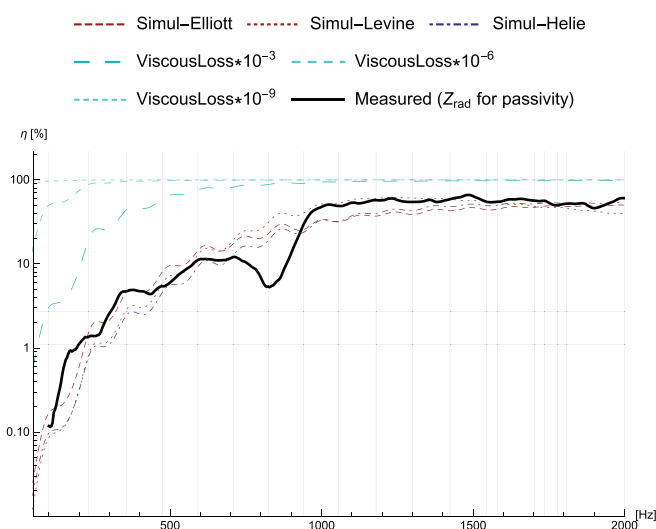

FIG. 10. (Color online) B♭-trumpet efficiency as derived from a basic set of measurements and a radiation impedance determined by the passivity condition, compared to simulations with different radiation models and loss factor.
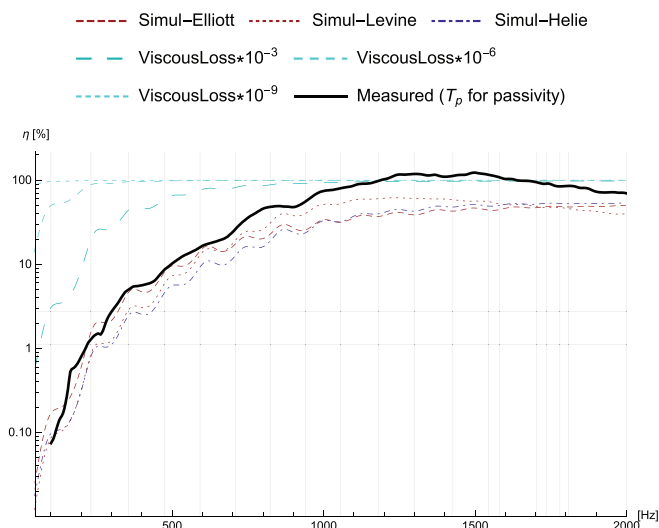
FIG. 11. (Color online) B♭-trumpet efficiency as derived from a basic set of measurements, a radiation impedance according to Helie–Rodet, and a free field pressure gain determined by the passivity condition, compared to simulations with different radiation models and loss factor.

available in the online repository. Similarities between the behavior of both instruments are striking. Only frequencies below and above the main playing range might seem to deviate, but it is not yet clear whether these differences are real or artifacts. Low frequency measurements are always very critical to leakage. And in the cutoff region, it is the radiation modeling and the plane or spherical wave assumption that have to be questioned.

V. DISCUSSION AND CONCLUSIONS

In a brass instrument's normal playing range, bells act as a rather good reflector for outgoing waves. Their reflection coefficient at the lowest resonances is very close to 1 and decreases steadily down to almost 0 for frequencies above cutoff. Therefore, it is expected that thermo-viscous
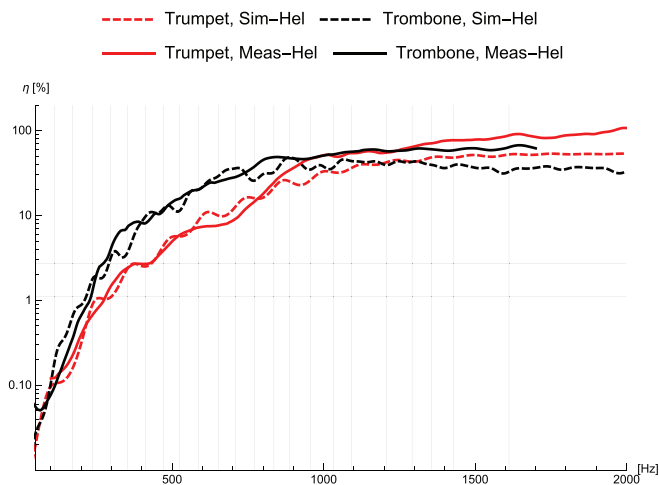

FIG. 12. (Color online) B♭-trumpet vs tenor trombone efficiency as derived from a basic set of measurements and a radiation impedance according to Helie–Rodet, compared to simulations based on the same radiation impedance model.

boundary layer losses will have a very pronounced effect on efficiency in the lowest frequency region. As frequencies rise higher, the bell becomes less and less of a barrier, so that sound power increasingly radiates instead of just recirculating inside the instrument. This increases the power efficiency until a point where everything is radiated and nothing is reflected at the bell. This frequency is called the cutoff frequency, and it marks the apex in the efficiency-vs-frequency curve. Beyond cutoff, no recirculation takes place, and sound waves travel along the length of the tube just once. But since frictional losses increase with frequency, the efficiency curve begins to decrease again beyond cutoff.

Theoretical as well as experimental efficiency curves exhibit this expected behavior quite well. In the playing range, these curves mainly reflect the ability of the bell to recirculate sound waves into strong standing waves at air column resonances. The other factor is the smoothness of the wall, which has some influence on the boundary layer thickness. Above cutoff, this is the only remaining factor. It should reveal itself in the negative slope of the efficiency curve beyond that point.

A third aspect might be hidden in the bumpiness caused by the sequence of resonances and anti-resonances. Since local flow maxima are swapped against local pressure maxima when going from a resonance to an anti-resonance, and since friction losses in turbulent flow require high velocities in the presence of bore discontinuities, they might affect resonances in a different way than anti-resonances, which could cause the ripples of the curve.

Clarifying these questions may be a topic of future research. Comparing efficiency curves of a variety of instruments and studying the differences in efficiency, in construction, and perhaps in the subjective assessment of the measured instrument's properties and quality aspects may help to develop a sound basis for a competent interpretation of such measurements in terms that are meaningful to musicians.

The proposed way of determining the system matrix and several related characteristics such as efficiency and pressure gain without the need of an anechoic chamber may help researchers but mainly makers and players of instruments to reliably assess acoustic characteristics of their instruments.

Introducing the passivity condition in the measurement process not only removes the necessity for making the most difficult measurement, it also is an indispensable check for data quality.

Future work might also explore ways to improve the reconstruction accuracy by questioning the assumption of spherical wave fronts and customizing the 3D-printed cap to better match the actual wave shape.

ACKNOWLEDGMENTS

J. Acoust. Soc. Am. **149** (4), April 2021

Kausel *et al.*   2709

paper but are part of an Acoustical Society of America (ASA) Proceedings of Meetings on Acoustics (POMA) publication (Kausel *et al.*, 2013).

ARTIM (**2021**). BIAS, https://www.artim.at (Last viewed April 6, 2021).

Bauer, B. B. (**1944**). "Notes on radiation impedance," J. Acoust. Soc. Am. **15**(4), 223–224.

Beauchamp, J. W. (**1980**). "Analysis of simultaneous mouthpiece and output waveforms of wind instruments," in *Proceedings of the 66th AES Convention*, May 6–9, Los Angeles, Audio Engineering Society Preprint No. 1626, pp. 1–8.

Beauchamp, J. W. (**1988a**). "Wind instrument transfer responses," J. Acoust. Soc. Am. **83**, S120.

Beauchamp, J. W. (**1988b**). "Wind instrument transfer responses," http://cmp.music.illinois.edu/beaucham/trombone/Beauchamp.ASA.s88.pdf (Last viewed April 6, 2021).

Berggren, M., Bernland, A., and Noreland, D. (**2018**). "Acoustic boundary layers as boundary conditions," J. Comput. Phys. **371**, 633–650.

Braden, A. C. P. (**2006**). "Bore optimisation and impedance modelling of brass musical instruments," Ph.D. thesis, University of Edinburgh, Edinburgh, UK.

Campbell, M. (**2004**). "Brass instruments as we know them today," Acta Acust. United Acust. **90**(4), 600–610.

Campbell, M., Gilbert, J., and Myers, A. (**2020**). *The Science of Brass Instruments* (Springer, New York).

Campbell, M., Myers, A., and Chick, J. (**2013**). "Influence of the bell profile of the trombone on sound reflection and radiation," Proc. Mtgs. Acoust. **19**, 035068.

Carson, J. R. (**1924**). "A generalization of the reciprocal theorem," Bell Syst. Tech. J. **3**(3), 393–399.

Chaigne, A., and Kergomard, J. (**2016**). *Acoustics of Musical Instruments* (Springer, New York).

Crandall, I. B. (**1926**). *Theory of Vibrating Systems and Sound* (Van Nostrand, New York).

Dalmont, J.-P. (**2001**). "Acoustic impedance measurement, Part I: A review," J. Sound Vib. **243**(3), 427–439.

Dickens, P., Smith, J., and Wolfe, J. (**2008**). "Improved precision in acoustic impedance measurements by using calibration loads without resonances," J. Acoust. Soc. Am. **123**(5), 3015–3015.

Elliott, S., Bowsher, J., and Watkinson, P. (**1982**). "Input and transfer response of brass wind instruments," J. Acoust. Soc. Am. **72**(6), 1747–1760.

Elliott, S. J., and Bowsher, J. M. (**1982**). "Regeneration in brass wind instruments," J. Sound Vib. **83**(2), 181–217.

Eveno, P., Dalmont, J.-P., Caussé, R., and Gilbert, J. (**2012**). "Wave propagation and radiation in a horn: Comparisons between models and measurements," Acta Acust. United Acust. **98**(1), 158–165.

Fletcher, N. H., and Rossing, T. D. (**1991**). *The Physics of Musical Instruments* (Springer-Verlag, New York), p. 179.

Fletcher, N. H., and Tarnopolsky, A. (**1999**). "Blowing pressure, power, and spectrum in trumpet playing," J. Acoust. Soc. Am. **105**(2), 874–881.

Gatland, H. B. (**2016**). *Electronic Engineering Applications of Two–Port Networks: Applied Electricity and Electronics Division* (Elsevier, New York).

Goedbloed, J. J. (**2006**). "Reciprocity and EMC measurements," Tijdschrift-NERG **71**(1), 15.

Helie, T., and Rodet, X. (**2003**). "Radiation of a pulsating portion of a sphere: Application to horn radiation," Acta Acust. United Acust. **89**(4), 565–577.

Hirschberg, A., Gilbert, J., and Wijnands, A. (**1996**). "Shock waves in trombones," J. Acoust. Soc. Am. **99**(3), 1754–1758.

Jansson, E., and Benade, A. (**1974**). "On plane and spherical waves in horns with non-uniform flare. II. Prediction and measurements of resonance frequencies and radiation losses," Acta Acust. United Acust. **31**(4), 185–202.

Kausel, W. (**2004**). "Bore reconstruction of tubular ducts from its acoustic input impedance curve," IEEE Trans. Instrum. Meas. **53**(4), 1097–1105.

Kausel, W., Beauchamp, J. W., and Carral, S. (**2013**). "Brass instrument power efficiency and the relationship between input impedance and transfer function," Proc. Mtgs. Acoust. **19**, 035069.

Kausel, W., Zietlow, D. W., and Moore, T. R. (**2010**). "Influence of wall vibrations on the sound of brass wind instruments," J. Acoust. Soc. Am. **128**(5), 3161–3174.

Keefe, D. H., Ling, R., and Bulen, J. C. (**1992**). "Method to measure acoustic impedance and reflection coefficient," J. Acoust. Soc. Am. **91**(1), 470–485.

Kemp, J. A. (**2002**). "Theoretical and experimental study of wave propagation in brass musical instruments," Ph.D. thesis, University of Edinburgh, Edinburgh, UK.

Leach, W. M., Jr. (**1996**). "A two-port analogous circuit and SPICE model for Salmon's family of acoustic horns," J. Acoust. Soc. Am. **99**(3), 1459–1464.

Levine, H., and Schwinger, J. (**1948**). "On the radiation of sound from an unflanged circular pipe," Phys. Rev. **73**, 383–406.

Mapes-Riordan, D. (**1993**). "Horn modeling with conical and cylindrical transmission-line elements," J. Audio Eng. Soc. **41**(6), 471–483.

Molloy, C. (**1948**). "Calculation of the directivity index for various types of radiators," J. Acoust. Soc. Am. **20**(4), 387–405.

Moore, T. R., Gorman, B. R., Rokni, M., Kausel, W., and Chatziioannou, V. (**2015**). "Axial vibrations of brass wind instrument bells and their acoustical influence: Experiments," J. Acoust. Soc. Am. **138**(2), 1233–1240.

Nagel, L. W. (**1975**). "Spice2: A computer program to simulate semiconductor circuits," Ph.D. dissertation, University of California, Berkeley, CA.

Nederveen, C. J. (**1969**). *Acoustical Aspects of Woodwind Instruments* (Frits Knuf, Amsterdam).

Rayleigh, J. W. S. B. (**1896**). *The Theory of Sound* (Macmillan, New York).

Silva, F., Guillemain, P., Kergomard, J., Mallaroni, B., and Norris, A. (**2009**). "Approximation of the acoustic radiation impedance of a cylindrical pipe," J. Sound Vib. **322**(1), 255–263.

Watkinson, P., and Bowsher, J. (**1982**). "Vibration characteristics of brass instrument bells," J. Sound Vib. **85**(1), 1–17.

Wolfram (**2021**). Wolfram Player, https://www.wolfram.com/player/ (Last viewed April 6, 2021).

Zorumski, W. E. (**1973**). "Generalized radiation impedances and reflection coefficients of circular and annular ducts," J. Acoust. Soc. Am. **54**(6), 1667–1673.